ChemComm



Cite this: DOI: 10.1039/c1cc11615k

www.rsc.org/chemcomm

COMMUNICATION

Superhydrophobic nanostructured silicon surfaces with controllable broadband reflectance†

Seong J. Cho, Taechang An, Jin Young Kim, Jungwoo Sung and Geunbae Lim*

Received 21st March 2011, Accepted 8th April 2011

DOI: 10.1039/c1cc11615k

Nanostructured superhydrophobic silicon surfaces with tunable reflectance are fabricated *via* a simple maskless deep reactive-ion etching process. By controlling the scale of the high-aspect-ratio nanostructures on a wafer-scale surface, surface reflectance is maximized or minimized over the UV-vis-IR range while maintaining superhydrophobic properties.

Unique functional nanostructures are generated routinely in nature. 1-3 For example, the lotus leaf and the legs of water striders⁴ have strong water-repulsive properties due to the chemical composition and the geometric micro- and nanostructures of their surfaces, which are referred to as superhydrophobic. A superhydrophobic surface possesses unique functionalities, such as self-cleaning⁵ and reduced drag force properties.^{6,7} An anti-reflective structure that mimics moth eyes is an example of a product that uses special functionalities of natural nanostructures.8 Sub-wavelength structures in moth eyes reduce reflectance over a broadband of wavelengths by generating a graded refractive index.9 Recently, researchers have tried to fabricate multi-functional nanostructures that combine two or more functionalities because of their potential use in industrial applications and scientific studies. For example, some nanostructured surfaces have been produced with both superhydrophobic and anti-reflective surfaces. 10-12 By applying these unique functionalities to photovoltaics or optical sensors, performance can be enhanced, and cost and required maintenance can be reduced. Along with research on multi-functional nanostructures, the ability to maximize or minimize the behaviors of functional nanostructures through structural modifications has received significant attention. 8,13-19 However, in contrast to single-functional nanostructures, the individual functionalities of multi-functional nanostructures are difficult to control because each functionality is affected simultaneously by the morphology of the nanostructure. Furthermore, there have been no reports on superhydrophobic surfaces with controllable high- to low-reflectance.

Here, we demonstrate superhydrophobic nanostructured silicon surfaces with tunable reflectance from high-reflectance (average relative reflectance of 92.7% *versus* a polished silicon surface in the ultraviolet–visible–infrared (UV–vis–IR) range of 200 to 3000 nm) to extremely low-reflectance (average relative reflectance of 0.78%) using high-aspect-ratio nanostructures. To our knowledge, 92.7% is the highest relative reflectance in superhydrophobic surfaces reported to date. ²⁰ The reflectance was tuned by controlling the length and morphology of the high-aspect-ratio nanostructures using a deep reactive-ion etching (DRIE) process with special conditions.

Fig. 1 shows schematic diagrams of superhydrophobic nanostructured silicon surfaces with high-reflectance and anti-reflectance using a tip-shaped nanostructure, also called nanograss. A high-aspect-ratio nanostructure is an optimized architecture that can control the wettability and reflectivity of a surface because the structure not only maximizes the roughness of the surface but also generates a graded refractive index profile. 4,21 We fabricated tip-shaped silicon nanograss (high aspect ratio: 5-50) on large areas, up to 4 in wafers, using DRIE based on the "black silicon" method.²² Experimental details are discussed in ESI†. The black silicon method can be used to fabricate nanostructures without preprocessing, such as lithography, because micro-masks are formed automatically on the silicon surface during plasma etching.²³ This simple process allowed us to produce nanostructures with high throughput at low cost. Additionally, the DRIE process is an integrated circuit (IC)-compatible process for solar cell and microelectromechanical system (MEMS) devices. The process is also adaptable for various crystal structures of silicon, including single-crystalline, polycrystalline, and amorphous silicon, ²⁴ and can be applied to structuring on three-dimensional (3D) surfaces as well as flat surfaces (Fig. S1 in ESI†). Using the black silicon method, we fabricated various scales of nanostructures on silicon surfaces by controlling the process time of the plasma etching. The length of the nanograss increased with increasing process time, whereas the density of the nanograss became saturated at about 40×10^7 cm⁻² (Fig. S2 in ESI†). Fig. 1B and C show the schematics and scanning electron microscopy (SEM) images of various scales of nanograss surfaces, such as short and sparse nanograss

a Department of Mechanical Engineering, Pohang University of Science and Technology (POSTECH), San 31, Pohang, Gyungbuk, 790-784, the Republic of Korea. E-mail: limmems@postech.ac.kr

b Department of Integrative Bioscience and Biotechnology, Pohang University of Science and Technology (POSTECH), San 31, Pohang, Gyungbuk, 790-784, the Republic of Korea

[†] Electronic supplementary information (ESI) available: Experimental details and data of fabricated nanostructures. See DOI: 10.1039/c1cc11615k

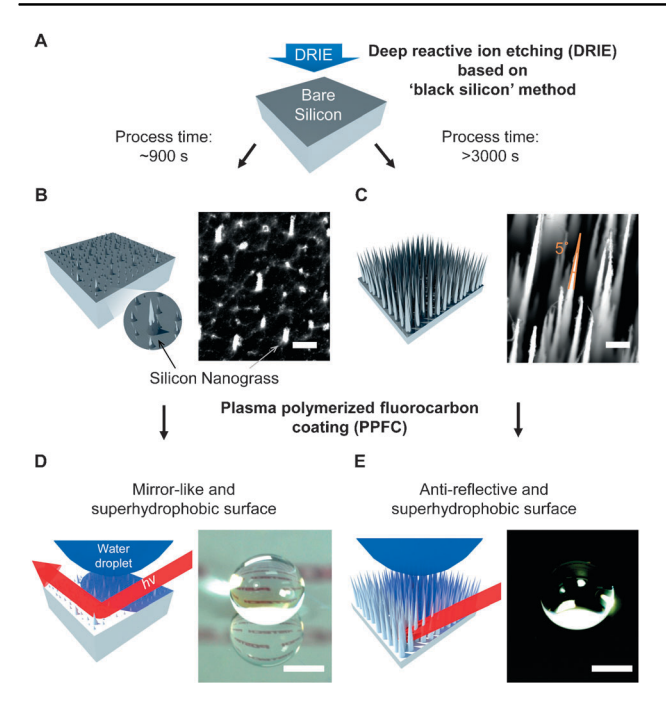


Fig. 1 Fabrication of superhydrophobic nanostructured silicon surfaces with high reflectance and anti-reflectance using tip-shaped nanostructures and images of the nanostructured surfaces. (A–C) Schematics of the fabrication of a high-aspect-ratio nanostructure, nanograss, using a deep reactive ion etching (DRIE) process based on the "black silicon" method and SEM images of a short and sparse nanograss surface and a long and packed nanograss surface. (D, E) After fluorocarbon polymer layer coating, both surfaces exhibited superhydrophobicity (contact angle, CA > 160°). The reflectance of the surfaces showed a stark contrast. In the case of a high-reflectance surface, the relative reflectance compared to a polished silicon surface was ~93% over the UV–Vis–IR range. However, an anti-reflective surface showed a relative reflectance of ~0.8%. Scale bars are 1 μm in (B, C) and 2 mm in (D, E).

surfaces, and long and packed nanograss surfaces. The nanograss that formed in the early stages of the etching process was short (<1 μm) and thin (average ~ 100 nm). As the process time increased, the nanograss grew longer while the base thickened. In the end, the long nanograss had a sharp-tip shape (the apex angle was $\sim 5^{\circ}$), and the width varied from 50 nm (apex) to 3 μm (base). After the etching process, a low-surface energy fluorocarbon polymer layer was deposited on the nanostructured surfaces by plasma polymerized fluorocarbon coating (PPFC) using the same system as the DRIE process to fabricate an anti-wetting surface. By modifying the scale of the nanograss, we fabricated superhydrophobic surfaces with various reflectance, as shown in Fig. 1D and E.

The size scale of the nanograss plays a crucial role in wettability and reflectivity. Fig. 2A shows the measured static contact angle (CA) and CA hysteresis, which is the differential between an advancing angle and a receding angle, as well as average relative reflectance in the UV–vis–IR range (200 to 3000 nm) *versus* a polished silicon surface according to the length of the nanograss. With increased length, the CA increased while reflectance decreased. The static CA increased smoothly until a length of 0.23 µm; at 0.75 µm, the static CA increased suddenly to 160°, and the hysteresis decreased to less than 6° because the wetting state changed from the Wenzel

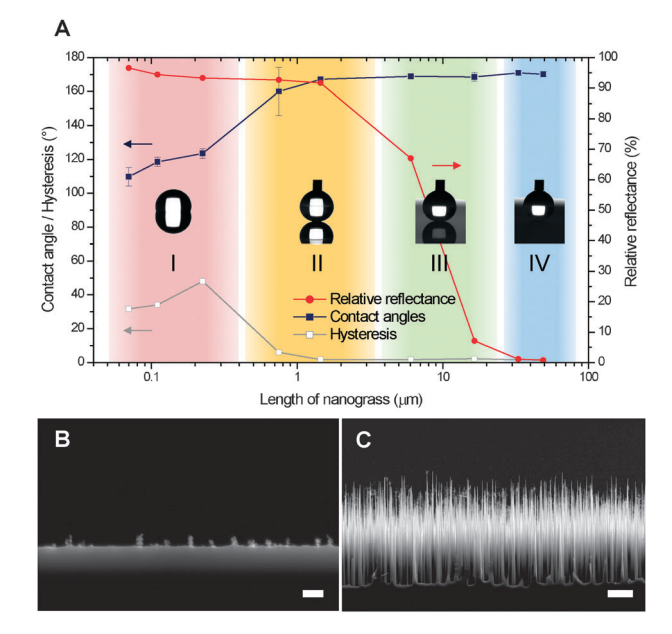


Fig. 2 (A) Wettability and reflectivity of the nanograss surface dependence on nanograss length. Although the wetting properties, such as static CA and CA hysteresis, changed rapidly at the submicron length scale, reflectance decreased for longer scales. Thus, by controlling the scale of the nanograss, various functional surfaces, including a high-reflectance and hydrophobic surface (region I), a high-reflectance and superhydrophobic surface (region III), and an antireflective and superhydrophobic surface (region IV), were fabricated. (B, C) Cross-sectional SEM images of region II (length: 0.75 μm) and region IV (length: 49 μm). Scale bars are 1 μm in (B) and 10 μm in (C).

state, in which a liquid droplet is impaled on rough surface features, to the Cassie state, in which a liquid droplet rests on a composite surface composed of solid and trapped air. 25 After the state change, the static CA increased gradually to 170° at a length of 49 μ m, and the hysteresis decreased to $\sim 2^{\circ}$. To determine the portion of the nanograss that supported a water droplet, we calculated an approximate penetration depth, which is the depth that the nanograss penetrated into the water droplet in the Cassie state, using Dorrer and Rühe's nanocone model. 13 The calculated penetration depth was ~ 70 nm for a drop with a 1 mm radius, a slope angle of 2.5° (half of the apex angle), and nanograss densities of 40×10^7 cm⁻² (the average density of the fabricated nanograss). Thus, an extremely small portion of the nanograss supported the water droplet, and the sub-micron nanograss surface exhibited superhydrophobicity. In contrast, reflectance displayed different tendencies. As the length of the nanograss increased, reflectance decreased gradually. Long nanograss ($> 30 \mu m$), in particular, had superior anti-reflectivity (<1%). The reflectance tendency was related to a refractive index profile.²⁶ Generally, a flat surface with a discontinuous refractive index profile has high reflectance, whereas a surface with a graded refractive index profile suppresses reflection. Therefore, to modify surface reflectance, the refractive index profile should be controlled. Fig. 2B shows cross-sectional SEM images of high-reflectance and superhydrophobic surfaces (length of 0.75 μm). The short and sparse nanograss generated a relatively discontinuous refractive index profile because the nanostructures on the surface had only sub-micrometre lengths

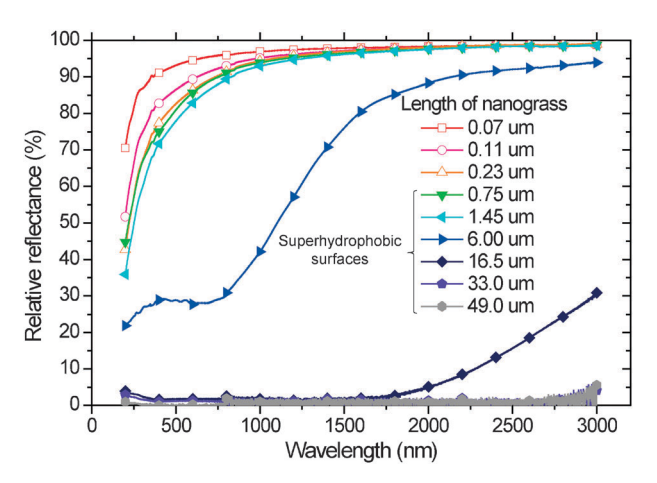


Fig. 3 Relative reflectance on the nanostructured surface with varied wavelength from the UV (200 nm) to the near IR (3000 nm) range at lengths of 0.07–49.0 μ m. Filled symbols denote superhydrophobic surfaces with CA values >150°, and open symbols denote non-superhydrophobic surfaces with CAs <150°.

and wide intervals (1–3 μ m). On the other hand, the tip-shaped nanostructures were long ($\sim 50 \mu m$), and the widths varied gradually (Fig. 2C). The continuous surface profile generated a graded effective refractive index profile, which can minimize reflectance. Thus, the morphology of the nanograss determines the surface reflectance as well as the wettability. Interestingly, the rapidly changing regions of the wetting and optical properties did not overlap, as shown in Fig. 2A. Hence, various functional silicon surfaces could be fabricated by controlling the length of the nanograss, i.e., a high-reflectance and hydrophobic surface (region I in Fig. 2A), a high-reflectance and superhydrophobic surface (region II), a low-reflectance and superhydrophobic surface (region III), and an anti-reflective and superhydrophobic surface (region IV). Regions II, III, and IV had superhydrophobic properties with various reflectance (relative reflectance of 92.7–0.78%).

The nanostructured surface with a graded refractive index profile exhibited tunable reflectance over a broadband wavelength region. Fig. 3 shows how the relative reflectance varied with the length of the nanograss in the UV-vis-IR range. The relative reflectance decreased as the wavelength narrowed and the nanograss length increased. In the UV region (200–400 nm), reflectance increased rapidly as wavelength increased. Among the superhydrophobic surfaces, the maximum relative reflectance was 75.0% at 400 nm, and the average minimum value of antireflective surfaces was 0.04% in the UV region. The maximum and minimum relative reflectance throughout the entire visible range (400-780 nm) was 90.5% at 780 nm and an average of 0.05\%, respectively. In the IR region (780 to 3000 nm), reflectance was greater than that in the UV-vis region; the maximum reflectance for the entire range was 98.7% at 3000 nm, and the minimum was an average of 0.9% over the entire measured IR region.

These light-sensitive and water-repulsive silicon surfaces can be used in solar cell devices and optical sensors because they have self-cleaning properties as well as improved light-absorbing performance over a wide wavelength region. In contrast, mirror-like and water-repulsive silicon surfaces can reflect broadband light, including the IR range, and minimize the

contact area between water and the silicon surface. Thus, the surfaces can minimize the absorption of energy from radiation through their exterior, conduction, or convection *via* water contact. It is believed that these unique properties can be used in thermal insulating devices or self-cleaning reflecting devices.

In summary, we demonstrated wafer-scale superhydrophobic silicon surfaces with controllable reflectance of broadband light using tip-shaped nanostructures by varying the morphology of the nanostructures on the surface. The thin and short nanostructured surfaces coated with a fluoropolymer layer displayed very high reflectivity (maximum relative reflectance: 98.7%) as well as superior superhydrophobicity. The surfaces with long and packed nanostructures exhibited anti-wetting properties and excellent anti-reflective properties in the UV–vis–IR range (<0.04% for certain ranges). The fabrication process based on maskless DRIE was simple and applicable to typical MEMS. We believe that the advantages of the method described here can be extended to solar cells, thermal insulation technology, optical sensors, and MEMS devices.

This research was financially supported by a grant to the MEMS Research Center for National Defense funded by the Defense Acquisition Program Administration. We are grateful for the support of Mr Kim at the National Center for Nanomaterials Technology.

Notes and references

- 1 W. Barthlott and C. Neinhuis, Planta, 1997, 202, 1.
- 2 C. G. Bernhard, Endeavour, 1967, 26, 79.
- 3 H. Ghiradella, Science, 1972, 178, 1214.
- 4 X. Gao and L. Jiang, Nature, 2004, 432, 36.
- 5 R. Blossey, Nat. Mater., 2003, 2, 301.
- 6 C. Choi and C. Kim, Phys. Rev. Lett., 2006, 96, 066001.
- 7 J. Kim and C. Kim, Proceedings of the 15th IEEE International Conference on Micro Electro Mechanical Systems, 2002, 479.
- 8 Y. Huang, S. Chattopadhyay, Y. Jen, C. Peng, T. Liu, Y. Hsu, C. Pan, H. Lo, C. Hsu, Y. Chang, C. Lee, K. Chen and L. Chen, *Nat. Nanotechnol.*, 2007, **2**, 770.
- 9 P. B. Clapham and M. C. Hutley, Nature, 1973, 244, 281.
- 10 W. Min, B. Jiang and P. Jiang, Adv. Mater., 2008, 20, 3914.
- 11 M. Kim, K. Kim, N. Y. Lee, K. Shin and Y. S. Kim, Chem. Commun., 2007, 2237.
- 12 Y. Xiu, L. Zhu, D. W. Hess and C. P. Wong, Nano Lett., 2007, 7, 3388.
- 13 C. Dorrer and J. Rühe, Adv. Mater., 2008, 20, 159.
- 14 X. J. Feng and L. Jiang, Adv. Mater., 2006, 18, 3063.
- C. Lee, S. Bae, S. Mobasser and H. Manohara, *Nano Lett.*, 2005, 5, 2438.
- 16 J. Zhu, Z. Yu, G. F. Burkhard, C. Hsu, S. T. Connor, Y. Xu, Q. Wang, M. McGehee, S. Fan and Y. Cui, *Nano Lett.*, 2009, 9, 279.
- 17 M. D. Kelzenberg, S. W. Boettcher, J. A. Petykiewicz, D. B. Turner-Evans, M. C. Putnam, E. L. Warren, J. M. Spurgeon, R. M. Briggs, N. S. Lewis and H. A. Atwater, *Nat. Mater.*, 2010, 9, 239.
- 18 Z. Fan, R. Kapadia, P. W. Leu, X. Zhang, Y. Chueh, K. Takei, K. Yu, A. Jamshidi, A. A. Rathore, D. J. Ruebusch, M. Wu and A. Javey, *Nano Lett.*, 2010, 10, 3823.
- 19 L. Sainiemi, V. Jokinen, A. Shah, M. Shpak, S. Aura, P. Suvanto and S. Franssila, *Adv. Mater.*, 2011, 23, 122.
- 20 L. Shen, J. Ji and J. Shen, Langmuir, 2008, 24, 9962.
- 21 L. Hu and G. Chen, Nano Lett., 2007, 7, 3249.
- 22 H. Jansen, M. Boer, R. Legtenberg and M. Elwenspoek, J. Micromech. Microeng., 1995, 5, 115.
- 23 M. Gharghi and S. Sivoththaman, J. Vac. Sci. Technol., A, 2006, 24, 723.
- 24 S. Koynov, M. S. Brandt and M. Stutzmann, *Appl. Phys. Lett.*, 2006, 88, 203107.
- 25 D. Quéré, Rep. Prog. Phys., 2005, 68, 2495.
- 26 S. Chattopadhyay, Y. Huang, Y. Jen, A. Ganguly, K. Chen and L. Chen, Mater. Sci. Eng., R, 2010, 69, 1.